BMC Cancer

RESEARCH Open Access

# Impact of celastrol on mitochondrial dynamics and proliferation in glioblastoma

Lei Liang[1,2†], Wenying Lv[3†], Gang Cheng[4], Mou Gao[4], Junzhao Sun[3], Ning Liu[5], Hanbo Zhang[1], Baorui Guo[1,4], Jiayu Liu[4], Yanteng Li[1,4], Shengqiang Xie[1], Jiangting Wang[6], Junru Hei[4] and Jianning Zhang[1,4*]

## Abstract

**Background** Targeting mitochondrial dynamics offers promising strategies for treating glioblastoma multiforme. Celastrol has demonstrated therapeutic effects on various cancers, but its impact on mitochondrial dynamics in glioblastoma multiforme remains largely unknown. We studied the effects of Celastrol on mitochondrial dynamics, redox homeostasis, and the proliferation.

**Methods** Mito-Tracker Green staining was conducted on U251, LN229, and U87-MG cells to evaluate the effects of Celastrol on mitochondrial dynamics. The Western blot analysis quantified the expression levels of mitochondrial dynamin, antioxidant enzymes, and cell cycle-related proteins. JC-1 staining was performed to discern mitochondrial membrane potential. Mitochondrial reactive oxygen species were identified using MitoSOX. The proliferative capacity of cells was assessed using Cell Counting Kit-8 analysis, and colony formation assays. Survival analysis was employed to evaluate the therapeutic efficacy of Celastrol in C57BL/6J mice with glioblastoma.

**Results** Our findings suggest that Celastrol (1 and 1.5 μM) promotes mitochondrial fission by downregulating the expression of mitofusin-1. A decrease in mitochondrial membrane potential at 1 and 1.5 μM indicates that Celastrol impaired mitochondrial function. Concurrently, an increase in mitochondrial reactive oxygen species and impaired upregulation of antioxidant enzymes were noted at 1.5 μM, indicating that Celastrol led to an imbalance in mitochondrial redox homeostasis. At both 1 and 1.5 μM, cell proliferation was inhibited, which may be related to the decreased expression levels of Cyclin-dependent kinase 1 and Cyclin B1. Celastrol extended the survival of GBM-afflicted mice.

**Conclusion** Celastrol promotes mitochondrial fission in glioblastoma multiforme cells by reducing mitofusin-1 expression, accompanying mitochondrial dysfunction, lower mitochondrial membrane potential, heightened oxidative stress, and decreased Cyclin-dependent kinase 1 and Cyclin B1 levels. This indicates that Celastrol possesses potential for repurposing as an agent targeting mitochondrial dynamics in glioblastoma multiforme, warranting further investigation.

**Keywords** Celastrol, Mitochondrial dynamics, Glioblastoma, Oxidative stress, CDK1 protein, Drug repurposing

†Lei Liang and Wenying Lv contributed equally to this work and are co-first authors.

*Correspondence:
Jianning Zhang
jnzhang2024_ll@163.com

Full list of author information is available at the end of the article

## Introduction

Glioblastoma multiforme (GBM) constitutes approximately 50% of all primary malignant brain tumors, making it the most common and aggressive form of brain cancer, with survival rates of 37.4% and 4.9% after one year and five years, respectively [1, 2]. Despite the development of new treatments such as direct intra-tumor drug delivery, molecular targeted therapy, tumor immunotherapy, and nanomedicine, achieving a complete cure remains challenging [3]. Therefore, exploring and developing effective therapeutic strategies for GBM from a novel perspective is crucial for advancing medical outcomes.

Mitochondria are pivotal in regulating numerous biological processes, such as oxidative phosphorylation, membrane potential generation, redox homeostasis, and the intrinsic apoptotic pathway, among others [4]. Growing evidence indicates that mitochondria are closely associated with cancer, including gliomas. For example, abnormal levels of mitochondrial reactive oxygen species (mROS), triggered by oncogene activation and hypoxia, help cancer cells survive by causing mutations in nuclear or mitochondrial DNA. Furthermore, mROS activate hypoxia-inducible factor 1 (HIF-1), shifting metabolism from oxidative phosphorylation to glycolysis, a phenomenon known as the 'Warburg effect,' by upregulating glycolytic enzymes. In addition to metabolic reprogramming, cancer cells alter their mitochondrial dynamics, primarily involving the balance of continuous fusion and fission processes of the mitochondrial membranes. To maintain the morphology, quantity, and functional integrity of mitochondria, their dynamics are essential. Unregulated mitochondrial fission can lead to fragmentation, which is often linked to various metabolic disorders and diseases. For example, mitochondrial fusion enhances ATP production, while its inhibition results in reduced oxidative phosphorylation and increased reactive oxygen species (ROS) production [5]. Excessive mitochondrial fission has been observed in various cancers, including brain tumors, lung cancer, breast cancer, and hepatocellular carcinoma [6]. The alterations mentioned above are crucial elements in the oncogenesis, progression, and therapy resistance of GBM [7–9]. Consequently, these adjustments make mitochondria a susceptible target for cancer therapies. Currently, novel therapeutic approaches targeting mitochondrial oxidative phosphorylation, the tricarboxylic acid cycle, and mitochondrial dynamics are being developed and investigated. These treatments have demonstrated promising efficacy in suppressing cancers [10–12]. A 2021 report indicates that pharmacological inhibition of mitochondrial fusion increases GBM sensitivity to temozolomide in both in vivo and in vitro experiments [13]. Unfortunately, there are currently no drugs targeting mitochondrial dynamics for the treatment of GBM available or in clinical trials [12].

Repurposing existing drugs is a convenient, cost-effective, and sensible approach to developing anti-tumor treatments that target mitochondrial dynamics [14]. Recently, Celastrol, also referred to as Tripterin or Tripterine, has garnered attention for its broad-spectrum efficacy as an anticancer agent with multi-targeted effects [15]. While studies have demonstrated Celastrol's anti-GBM effects through ROS/JNK activation and Akt/mTOR inhibition, its impact on mitochondrial dynamics remains under-researched [16–18]. In a non-small-cell lung cancer study, researchers discovered that erastin and Celastrol together boosted ROS production and induced mitochondrial fission [19]. This suggests that Celastrol may have the potential to affect mitochondria in GBM and regulate mitochondrial dynamics, possibly serving as a candidate for repurposing existing drugs to target these dynamics.

To test this hypothesis, we examined the effects of Celastrol on mitochondrial dynamics. We found that Celastrol can promote the development of mitochondrial dynamic homeostasis in the direction of fission, and that the reduction of mitofusin-1 (Mfn1) expression may mediate this process. We further investigated the effects of Celastrol on mitochondrial functionality, redox homeostasis, and the proliferation of GBM cells. The findings demonstrated that the reduction in mitochondrial membrane potential ($\Delta\psi M$) and the elevation in oxidative stress were accompanied by an increase in mitochondrial fission. Furthermore, Celastrol effectively suppressed the proliferation of GBM cells and extended survival duration in murine models of GBM. Our research indicates that Celastrol exhibits potential for repurposing as a therapeutic agent targeting mitochondrial dynamics in GBM, warranting further investigation.

## Materials and methods

### General reagents

Celastrol (HY-13067) was provided by MedChemExpress and dissolved in dimethyl sulfoxide (DMSO) to create a 1 mM stock solution. Different concentrations of the Celastrol working solution were obtained by diluting the stock solution with complete medium. 0.1% DMSO diluted in the same medium was used to treat the cells in the control groups.

### GBM cell lines

The Laboratory of Ning Liu provided the human GBM cell lines U251 and LN229, as well as the mouse GBM cell line GL261. We purchased the U87-MG cell line from EallBio Life Sciences (Beijing, China). We selected these three recognized GBM model cell lines based on the research conducted by Cha et al. [18]. Cells were

cultured in Dulbecco's Modified Eagle Medium (8123441, Thermo Fisher, USA) supplemented with 10% heat-inactivated, filter-sterilized fetal bovine serum (DX-1001, Daxi, China) and 100 U/mL penicillin and 100 μg/mL streptomycin(CA0075, Leagene, China). This medium mixture was referred to as a complete medium. Cells were cultured at 37 °C with 5% $CO_2$ in a carbon dioxide incubator (3111, Thermo Fisher, USA).

#### Analyses of cell viability and IC50 curve fitting

Cell viability of U251, LN229, U87-MG, and GL261 was assessed using the CCK-8 assay kit (40203ES76, Yeasen, China), following the manufacturer's instructions. Cells were seeded at $1 \times 10^4$ per well in a 96-well plate and treated with Celastrol at 1.0 μM, 1.5 μM, 2.0 μM, and 3.0 μM for 24 hours. In choosing the concentration of Celastrol, we draw upon the research conducted by Cha et al. regarding the growth curves of GBM cells at various concentrations [18]. A 1:10 dilution of the CCK-8 solution was added to the cells and incubated for 1 hour. The relative cell viability was assessed using a microplate reader (HBS-1096A, DeTie, China) by measuring optical density (OD) at 450 nm and calculating the ratio of the experimental OD to the mean OD of the control group. To rationally determine the appropriate drug concentration range for our study, we used the 'Inhibitor versus normalized response using the variable slope' module within the nonlinear fitting function of GraphPad Prism 8.0.2 (GraphPad Software, USA) to model the IC50 curve, thereby elucidating the relationship between drug concentration and response.

#### Cell imaging in bright field view

GBM cells were seeded in 6-well plates at 75% confluence and incubated overnight at 37 °C with 5% $CO_2$. They were exposed to Celastrol at 1.0 μM, 1.5 μM, and 2.0 μM for 24 h. Images were taken with a microscope (CKX41, OLYMPUS, Japan) in bright field view.

#### Analyses of colony formation

$5 \times 10^2$ LN229 and GL261 cells were plated in a 6-well plate and exposed to 1.0 μM Celastrol for 8 h. Subsequently, they were permitted to incubate in complete DMEM for a duration of 7 to 14 days. A 0.1% crystal violet solution was used to stain the cells after they were fixed with 4% paraformaldehyde. The Fiji software (version 1.54f) was used to analyze images. A colony is defined as an aggregation of at least 50 cells. Colony formation efficiency was calculated by dividing the number of clones by 500 and multiplying by 100% [20].

#### Mitochondrial morphological imaging

$1 \times 10^4$ U251, LN229, and U87-MG cells were seeded on a glass-bottom petri dish (801002, NEST, China) and cultured overnight. Celastrol was administered to cells at concentrations of 1.0 and 1.5 μM for 24 h. According to the reagent instructions, cells were incubated with 250 nM Mito-Tracker Green FM (M7514, Invitrogen, UK) for 30 min at 37 °C. Three washes of DMEM (8123441, Thermo Fisher, USA) were conducted before and after staining. High-resolution mitochondrial images were obtained using a confocal laser scanning microscope (TCS SP5, Leica; Wetzlar, Germany).

#### Mitochondrial measurements

Micrographs showing stained mitochondria were processed using the MiNA 2.0.0 plug-in (available at https://github.com/StuartLab) [21] of Fiji software to acquire images of contoured mitochondria. These images are named as 'mitochondrial skeleton'. We measured mean mitochondrial length and mean mitochondrial area of skeletal images using MiNA and the Analyze Particles program of Fiji for cells from three independent biological replicates.

#### Western blot analysis

$2 \times 10^6$ U251 and LN229 cells were seeded in 6 cm Petri dishes and cultured overnight. After treatment with Celastrol at concentrations of 1 and 1.5 μM for 24 h, the cells were digested with 0.25% trypsin (CC0139, Leagene, China), suspended in PBS, centrifuged at 300 x g for 5 min, and collected in EP tubes. Then we lysed the cells on ice for 30 min using RIPA buffer containing 1% phenylmethanesulfonyl fluoride (PS0012, Leagene, China) and 1% protease inhibitor (PI0015, Leagene, China). The whole cell lysate was obtained by centrifuging the supernatant at 12,000 x g for 15 min. Following the quantification of protein concentration using the BCA Protein Assay Kit (PT0001, Leagene, China), samples were mixed with SDS loading buffer (PE0025, Leagene, China) and subjected to thermal denaturation at 100 °C for 15 min. Samples from each group were allocated to three distinct lanes, with each lane serving as a biological replicate. A protein sample of 40 μg was loaded into each lane. Subsequently, vertical electrophoresis was performed using a vertical electrophoresis tank (DYCZ-24KS, LiuYi, China) with a 12.5% SDS-polyacrylamide gel (AQ139, Aoqing, China). Subsequently, the proteins were electrotransferred onto a nitrocellulose membrane or a PVDF membrane using the wet transfer method. The membrane was blocked at room temperature for 1 h using a 5% skimmed milk solution in Tris-buffered saline with 0.1% Tween 20. Primary antibodies [anti-Mfn1 (bsm-60386 M, Bioss, China), anti-MFF (ab129075, Abcam, UK), anti-Fis1 (ab229969, Abcam, UK), anti-Nrf2 (R380773, Zenbio, China), anti-SOD1 (R25829, Zenbio, China), anti-HMOX1 (R380753, Zenbio, China), anti-CDK1 (ab133327, Abcam, UK), anti-Cyclin B1

(ab181593, Abcam, UK), and anti-β-actin (TA-09, ZSGB-BIO, China)] were diluted 1:1000 and incubated overnight at 4 °C on the membranes for further analysis. We incubated the membranes with horseradish peroxidase (HRP)-conjugated secondary antibodies [goat anti-rabbit IgG (GB23303, Servicebio, China), goat anti-mouse IgG (GB23301, Servicebio, China)] at a dilution of 1:2000 to 1:4000 for 1-1.5 h at room temperature. Following this, the immunoblot strips were visualized using a chemiluminescence imager (K4600, Jiapeng, Shanghai, China) after treatment with an enhanced chemiluminescence (ECL) reagent (PW0111, Leagene, China). Using Fiji, the relative expression levels of the target protein were analyzed and normalized to the loading control (β-actin).

#### Measuring mitochondrial membrane potential

U251, LN229, and U87-MG cells ($8 \times 10^4$) were plated overnight in 24-well plates and treated with 1 μM and 1.5 μM Celastrol for 24 h. A protocol provided by the manufacturer was followed to determine the ΔψM using JC-1 dye (CT0045, Leagene, China). In terms of experimental operations and result presentation, we learned from the methods of Yang et al. [22]. In summary, following the two washes with PBS, the cells were completely immersed in 0.5 mL of JC-1 staining solution and incubated at 37 °C in an atmosphere containing 5% $CO_2$ for 20 min. Subsequently, the cells underwent two washes with the pre-cooled JC-1 buffer, after which 1 mL of DMEM was added. The cells were then observed and imaged using an inverted fluorescence microscope (CKX41, OLYMPUS, Japan). Fluorescence images were analyzed with Fiji to evaluate fluorescence intensity and assess ΔψM by comparing red and green fluorescence values.

#### mROS measurement

Cell preparation and processing follow the same steps as ΔψM measurement. We measured mROS using MitoSOX Red (HY-D1055, MedChemExpress, USA) [23]. A 5 mM stock solution was prepared by dissolving 50 μg of MitoSOX Red in 13 μL of DMSO, then diluted to a 5 μM working solution with DMEM. Each well received 200 μL of this solution and was incubated at 37 °C for 30 min, followed by three washes with DMEM. Next, 500 μL of DAPI (02.10538-1, EallBio, China) solution (10 μg/mL in DMEM) was added to each well and incubated at 37 °C for 20 min. After three washes with PBS, 1 mL of DMEM was added, and imaging was conducted using a fluorescence microscope (DP71, OLYMPUS, Japan). Images were analyzed using Fiji, and the production of mROS was quantified by measuring the intensity of red fluorescence.

#### Allograft model in vivo

Eight-week-old male C57BL/6J mice were obtained from Sipeifu (Beijing) Biotechnology Co., Ltd. and housed at the Institute of Analysis and Testing, Beijing Academy of Science and Technology. The mice were kept at room temperature with ad libitum access to food and water, under a 12-hour light/dark cycle. Routine maintenance feed, as well as sterilized drinking water, was provided to them on a regular basis each term. To establish allograft model [24], GL261 cells were cultured with complete DMEM. Mice were subcutaneously injected with $5 \times 10^6$ cells in 100 μL DMEM in the right hind leg. On the eighth day after cell injection, a subcutaneous tumor mass reliably formed. Five mice were randomly allocated to one of two experimental conditions based on tumor volume: the Celastrol treatment group or the control group (DMSO treatment). Celastrol, diluted in PBS to a concentration of 100 μM, was administered to the mice in the Celastrol group at a dosage of 1 mg/kg via intraperitoneal injections [25] every other day for a total of three administrations. The control group mice received injections of 1% DMSO diluted in PBS. Tumor size was measured with a caliper every two days following the initial treatment administration. A mathematical formula was used to approximate the tumor mass [(large diameter) × (small diameter)$^2 \times 0.5$] [26]. Mice were euthanized via cervical dislocation when tumor volume reached 2000 $mm^3$ or when the largest diameter was 20 mm. Animal euthanasia procedures were conducted in accordance with the 2020 American Veterinary Medical Association (AVMA) Guidelines. The time between the initiation of administration and the end of euthanasia was defined as the survival time.

#### Statistics

Data entry, collation, and calculation were carried out with Microsoft Office Excel 2021 (Microsoft, USA). Statistical analysis was performed using GraphPad Prism 8.0.2, with data from three independent experiments expressed as the mean ± SEM. A one-way ANOVA was used for multiple independent quantitative data sets, assuming normality and homogeneity of variance. Post-tests were conducted only when the results of the tests were statistically significant. For post-hoc analysis following one-way ANOVA, Tukey's tests were employed. For the analysis of two independent quantitative datasets, a two-tailed independent samples t-test was employed if the datasets passed both the normality test and the homogeneity of variance test. Kaplan-Meier survival curves were analyzed using the Log-rank test. P-values below 0.05 were considered statistically significant. All illustrations were drawn with Adobe Illustrator CC 2021, version 25.0 (Adobe, USA).

## Results

### Celastrol restrains the viability of GBM cells

After 24 h of treatment with Celastrol, U251, LN229, and U87-MG cells exhibited IC50 values of 1.494 μM, 2.999 μM, and 3.159 μM, respectively (Fig. 1a, b; Additional file 1a). After Celastrol concentrations exceeded 1 μM, the viability of cells decreased in a concentration-dependent manner (Fig. 1c, d; Additional file 1b). Meanwhile, alterations of the morphological changes were basically consistent with cell viability (Fig. 1e; Additional file 1c). The results indicated that within the concentration range of 1 μM to 2 μM, there was a significant reduction in cell viability and a marked inhibition of cell proliferation. Consequently, this concentration range was selected for further investigation. To examine the effects of Celastrol on mitochondria while maintaining relatively high cell viability, we focused our studies on concentrations of 1 μM and 1.5 μM.

### Celastrol promotes mitochondrial fission in human GBM cells

Our initial objective was to investigate the impact of Celastrol on mitochondrial dynamics in human GBM cells. We treated U251, LN229, and U87-MG cells with Celastrol at concentrations of 1.0 μM, and 1.5 μM for 24 h. After that, we observed the morphology of mitochondria during the experimental procedure (Fig. 2a). The results indicated that mitochondria in U251, LN229, and U87-MG cells changed from long rods to short rods, dots, and small rings (Fig. 2b, c; Additional file 2a). Interestingly, through clonal formation experiments, we observed a significant inhibition in the proliferation of LN229 cells following treatment with Celastrol at concentrations of 1 μM and 1.5 μM for a duration of 8 h (Additional file 2 g-j). Consequently, we hypothesize that the effects of Celastrol on mitochondrial dynamics may manifest as early as 8 h post-treatment. Experimental

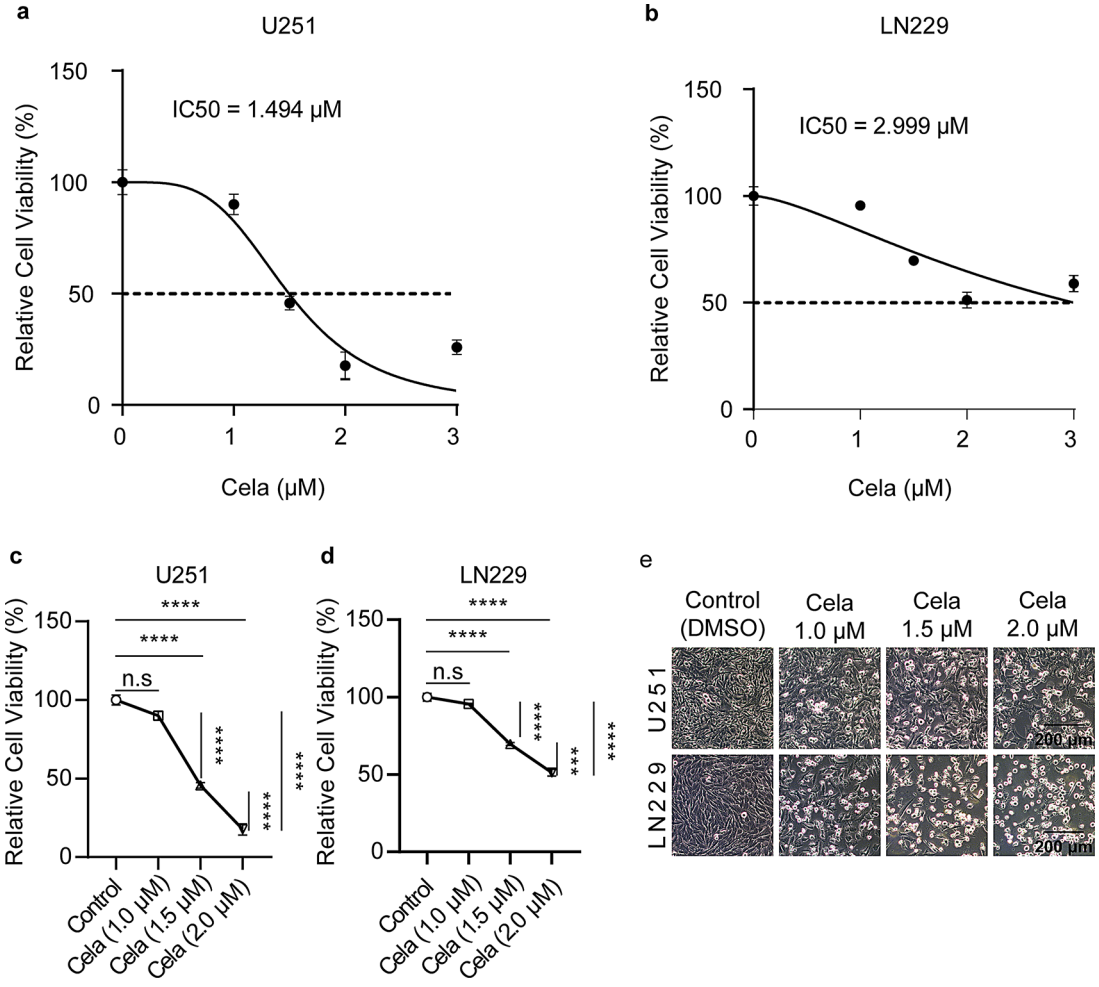


**Fig. 1** Celastrol restrains the viability of GBM cells. (**a**, **b**) IC50 curves of U251 and LN229 cells inhibited by Celastrol. (**c**, **d**) Impact of Celastrol on U251 and LN229 cell viability. The viability of cells challenged with Celastrol was measured by CCK8 assay. A one-way ANOVA was employed to conduct statistical inference on the differences between groups. $^{***}p < 0.001$, $^{****}p < 0.0001$, $^{n.s}p > 0.05$. Data are mean ± SEM. (**e**) Representative morphology micrographs of U251 and LN229 cells exposed to Celastrol. The scale bar represents a length of 200 μm. Abbreviation: Cela = Celastrol

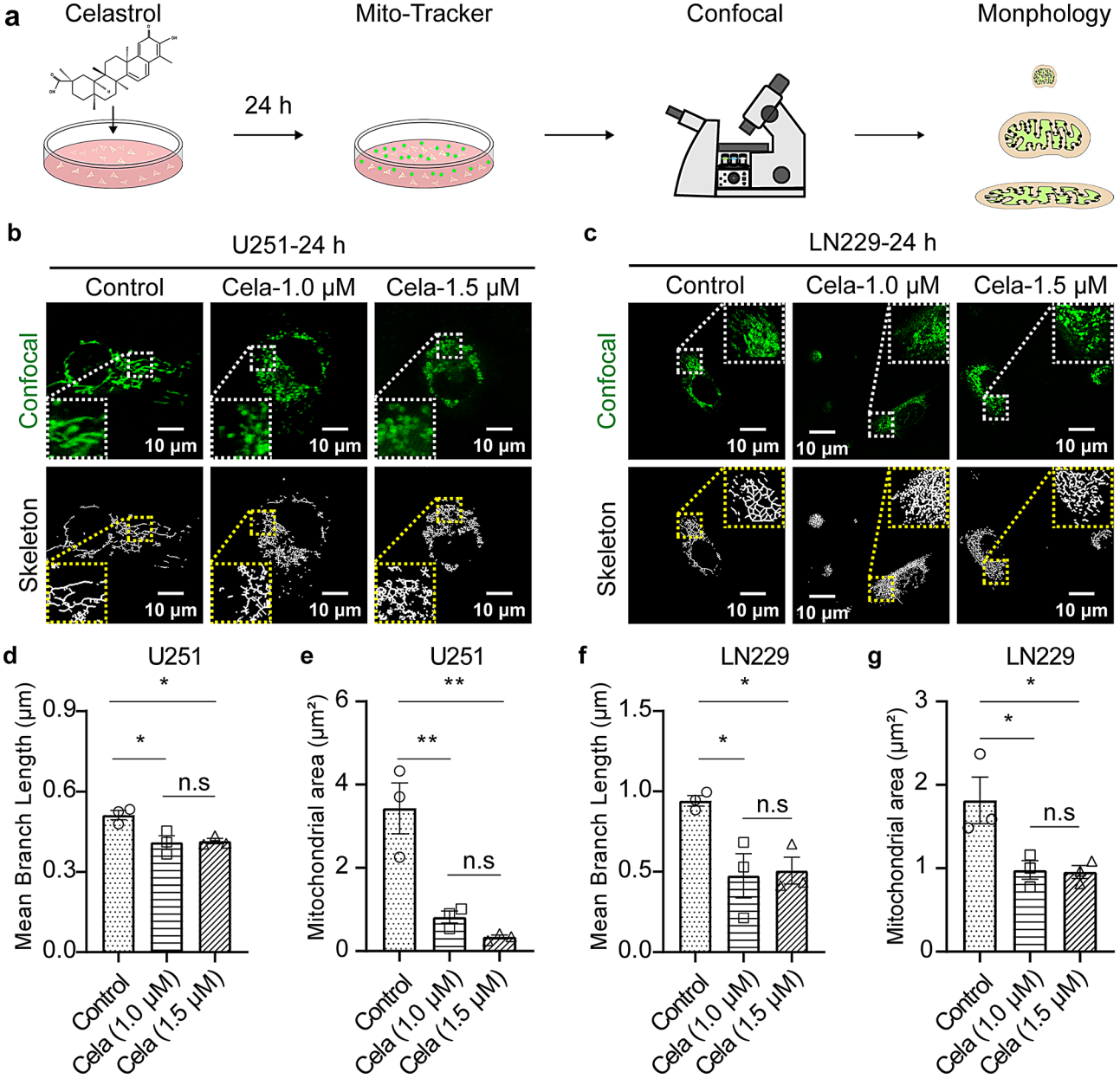


**Fig. 2** Celastrol facilitates mitochondrial fission. (**a**) Experimental procedure used to investigate the impact of Celastrol on the mitochondrial morphology of human GBM cells. (**b**, **c**) Confocal micrographs of mitochondria in U251 and LN229 cells exposed to Celastrol. The micrographs represent $n = 3$ independent experiments. "Confocal" refers to the original confocal micrographs, while "Skeleton" denotes the corresponding mitochondrial skeleton graphs generated by Fiji. The scale bar represents a length of 10 μm. (**d**, **e**, **f**, **g**) Quantification of mean mitochondrial length and mean mitochondrial area in U251 and LN229 cells exposed to Celastrol. Data are expressed as mean ± SEM from three independent biological replicates, with statistical analysis performed using one-way ANOVA. $^{*}p < 0.05$, $^{**}p < 0.01$, $^{n.s}p > 0.05$. Abbreviation: Cela = Celastrol

findings corroborated this hypothesis, revealing that the mitochondrial morphology in LN229 cells exhibited similar characteristics after an 8-hour exposure to Celastrol, as observed following a 24-hour exposure (Additional file 2d). Celastrol notably decreased mean mitochondrial length and area at concentrations of 1.0 μM and 1.5 μM, with no significant difference between these two concentrations (Fig. 2d-g; Additional file 2 b, c, e, f).

These findings demonstrate that Celastrol promotes mitochondrial fission in human GBM cells at concentrations of 1.0 μM or higher. However, increasing the concentration of Celastrol from 1.0 μM to 1.5 μM did not further increase the degree of mitochondrial fission.

### Mfn1 is downregulated by Celastrol in human GBM cells

In mammalian cells, Dynamin-related protein 1 (Drp1) facilitates outer mitochondrial membrane (OMM)

fission, whereas Mfn1 regulates OMM fusion. Drp1 requires interaction with receptor proteins on OMM, such as mitochondrial fission factor (MFF) and Fission 1 (Fis1) [27], for optimal functioning. In order to understand Celastrol's effect on mitochondrial dynamics-related proteins, we performed Western blot to quantify the expression levels of Mfn1, MFF, and Fis1 in U251 and LN229 cell lines (Fig. 3a, e). For U251 cells, the results indicated that the expression of Mfn1 decreased significantly at concentrations of 1.0 μM and 1.5 μM (Fig. 3b). Moreover, for LN229 cells, the expression of Mfn1 diminished markedly only at a concentration of 1.5 μM (Fig. 3f). However, MFF and Fis1 in the two types of cells did not exhibit significant alterations at any concentration (Fig. 3c, d, g, h). These results indicate that Mfn1 is downregulated by Celastrol in human GBM cells.

**ΔΨM declines in response to Celastrol in human GBM cells**

In mitochondrial electron transport chains, hydrogen ions are pumped from the matrix into the intermembrane space, creating the ΔψM. Maintaining mitochondrial oxidative phosphorylation and generating adenosine triphosphate require normal ΔψM levels. Thus, ΔψM serves as an indirect indicator of mitochondrial ATP synthesis capability. The shape of mitochondria may directly affect biological energy production. For instance, longer mitochondria are sometimes linked to more efficient ATP production [28]. We then evaluated the changes in ΔψM in mitochondria that were shortened by Celastrol using JC-1 staining (Fig. 4a, c; Additional file 3a; Additional file 4a, c).

After a 24-hour treatment with Celastrol, the red-to-green fluorescence intensity ratios, which reflect overall ΔψM levels, significantly decreased at 1 μM, 1.5 μM and 2 μM (Fig. 4b, d; Additional file 3b; Additional file 4b, d).

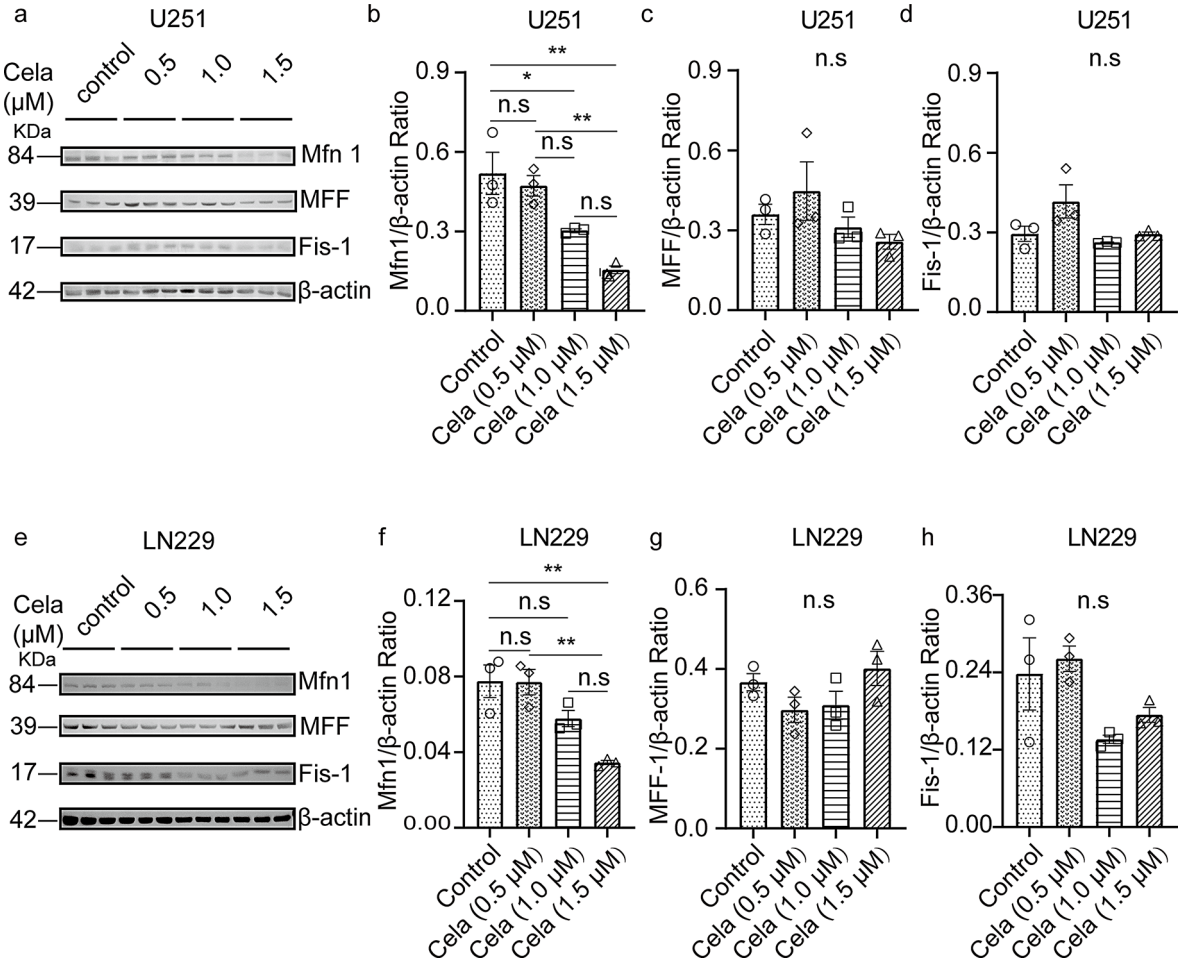


**Fig. 3** Mfn1 is downregulated by Celastrol in human GBM cells. (**a**) A representative Western blot analysis of Mfn1, MFF, and Fis-1 in U251 cell lysates. The cells were treated with Celastrol, and protein loading was normalized using β-actin as a control. (**b**, **c**, **d**) Quantifications of the protein expression levels shown in panel (a). (**e**) A representative Western blot analysis of Mfn1, MFF, and Fis-1 in LN229 cells treated with Celastrol. (**f**, **g**, **h**) Quantifications of the data presented in panel (**e**). The data, based on three independent replicates, are expressed as the mean ± SEM and analyzed using one-way ANOVA. $^{*}p < 0.05$, $^{**}p < 0.01$, $^{n.s}p > 0.05$. Abbreviation: Cela = Celastrol; Mfn1 = mitofusin-1; MFF = mitochondrial fission factor; Fis-1 = fission 1

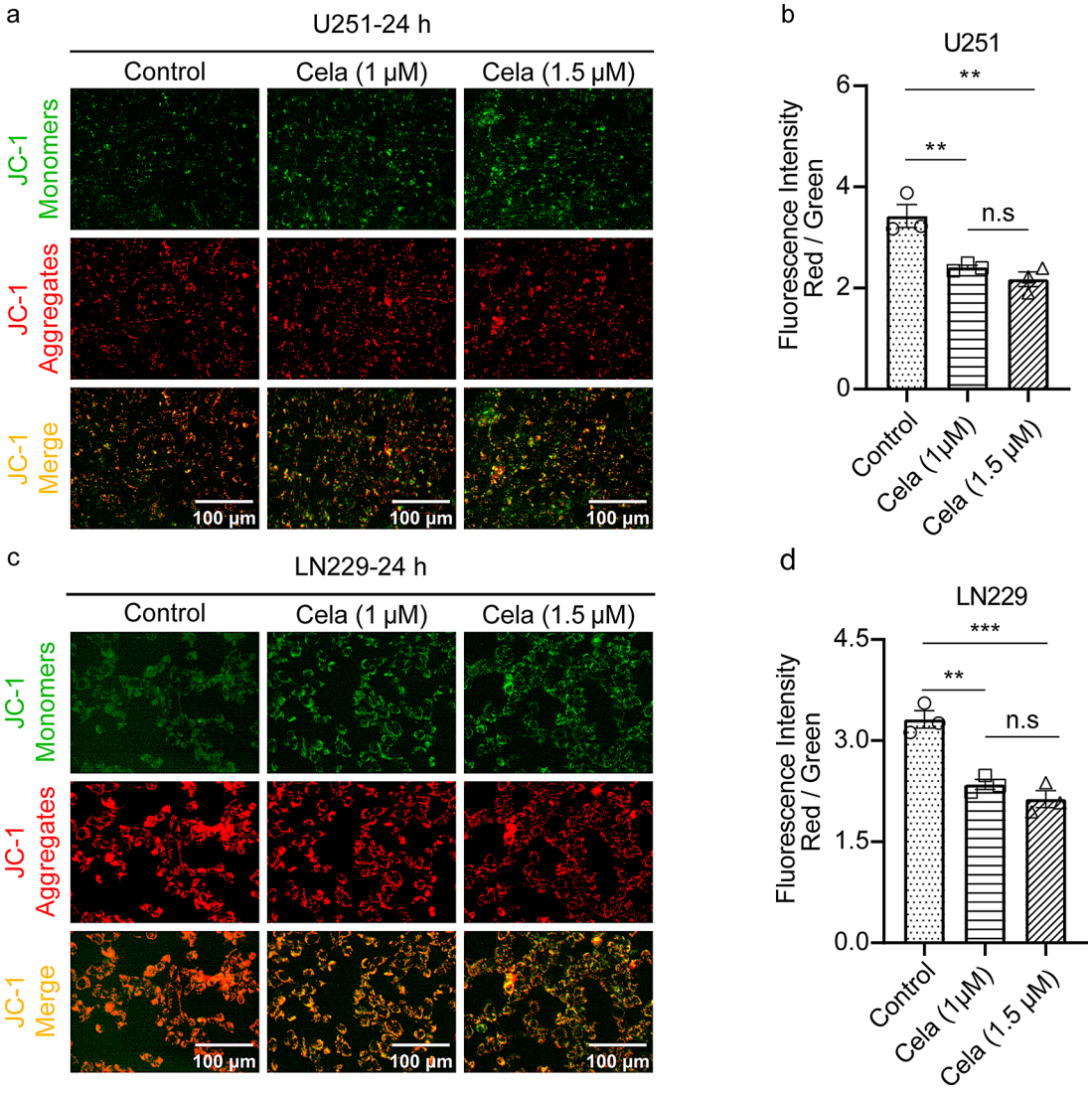


**Fig. 4** ΔψM is declined by Celastrol. (**a**, **c**) Fluorescence micrographs of ΔψM of U251 and LN229 cells treated with Celastrol (1 μM, 1.5 μM). ΔψM was observed after JC-1 staining. Micrographs represented 3 independently replicate experiments. The scale bar represents a length of 100 μm. (**b**, **d**) Quantifications of ΔψM. The ΔψM level is indicated by the ratio of the fluorescence intensity of aggregates to that of monomers of JC-1. Based on three independent replicates, the data represents the mean ± SEM. Statistics were conducted via one way ANOVA. $^{**}p < 0.01$, $^{***}p < 0.001$, $^{n.s}p > 0.05$. Abbreviation: Cela = Celastrol; ΔψM = mitochondrial membrane potential

Additionally, in LN229 cells, the degree of overall ΔψM decline was found to be concentration-dependent. These results demonstrate that ΔψM is decreased by Celastrol in human GBM cells. It was also indirectly implied that Celastrol caused damage to mitochondrial function.

### Celastrol leads to imbalance of mitochondrial redox homeostasis in human GBM cells

Growing evidence suggests a connection between mitochondrial dynamics and mitochondrial redox homeostasis [29]. It is well known that ROS, mainly involving in superoxides and hydrogen peroxides, is the major player in cellular redox homeostasis. In addition, about half of total ROS is associated with mitochondria. If ROS cannot be eliminated in time by the antioxidant system within cells, it can destroy important biological macromolecules and cellular structures. Hence, we wanted to further survey the effects of Celastrol on mitochondrial redox homeostasis in human GBM cells.

In U251, LN229, and U87-MG cells, mROS production significantly increased 24 h after treatment with 1.5 μM Celastrol, while 1 μM exposure showed no significant impact (Fig. 5a-d; Additional file 5a, b). This result aligns with the characteristic behavior of ΔψM binding, where increased impairment of mitochondrial function correlates with elevated production of mROS.

NF-E2-related factor 2 (Nrf2), the principal regulator of the cellular antioxidant response, mediates

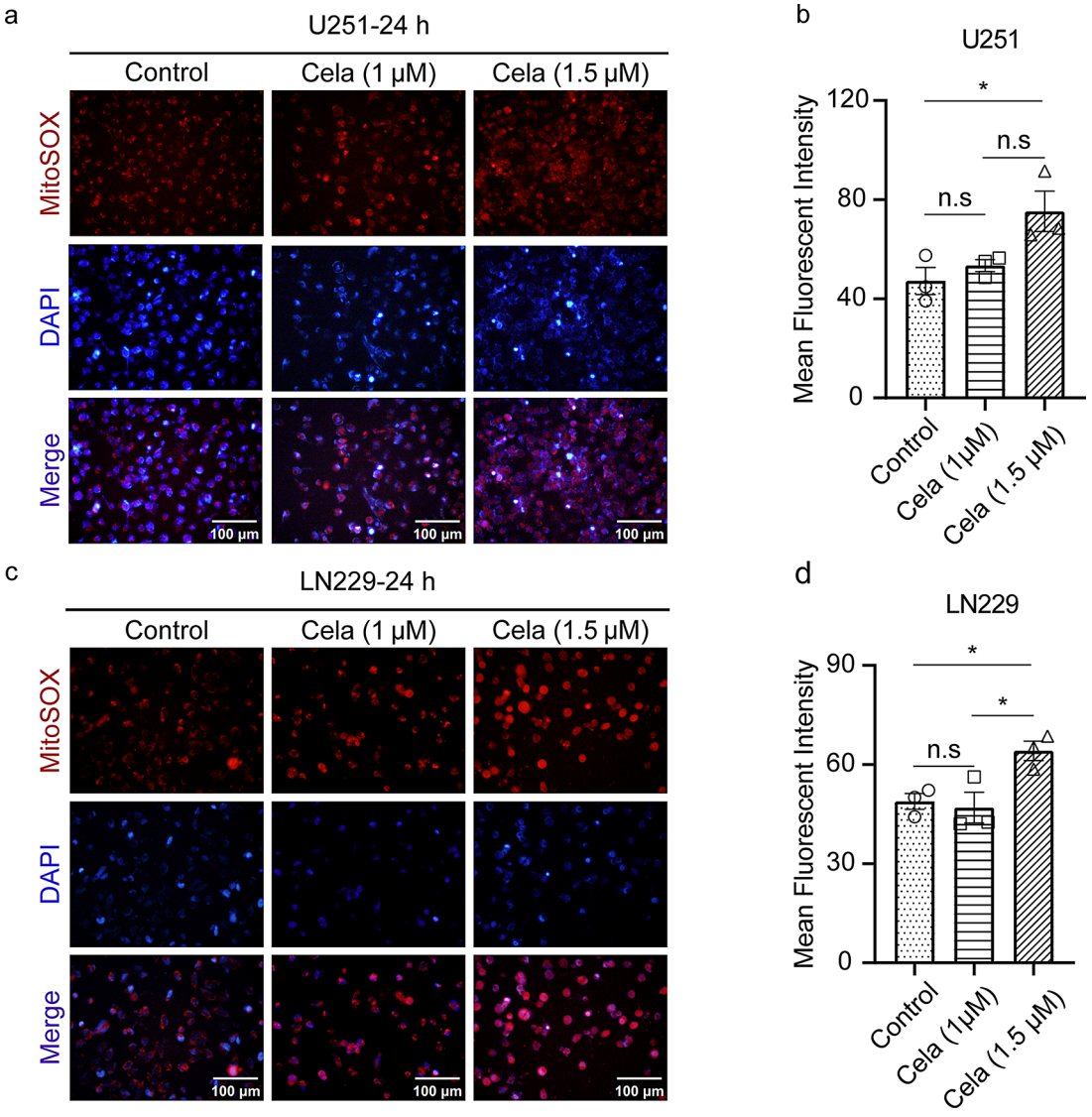


**Fig. 5** Celastrol resulted in increased mROS production. (**a**, **c**) Fluorescence micrographs of mROS in U251 and LN229 cells treated with Celastrol (1 μM, 1.5 μM). MitoSOX with red fluorescence indicating mROS in cells was observed immediately after staining. DAPI staining shows the nucleus. Micrographs represented 3 independently replicate experiments. The scale bar represents a length of 100 μm. (**b**, **d**) Quantifications of mROS levels in U251 and LN229 cells. A one-way ANOVA was employed to conduct statistical inference on the differences between groups. $^{*}p < 0.05$, $^{n.s}p > 0.05$. Data are expressed as mean ± SEM from three independent biological replicates. Abbreviation: mROS = mitochondrial reactive oxygen species; Cela = Celastrol

mitochondrial and NADPH oxidase-derived ROS and is considered essential for facilitating the adaptive survival response [30]. As vital parts of the antioxidant system in cells, SOD and HMOX1 play important roles in cleaning ROS. At the same time, HMOX1 is also an important downstream molecule of the Nrf2-ARE pathway [31, 32]. To elucidate the status of the intracellular antioxidant defense system following Celastrol treatment, the expression levels of the proteins Nrf2, HMOX1, and SOD1 were assessed using Western blot analysis (Fig. 6a, e). The results indicated that Celastrol treatment did not significantly alter Nrf2 expression in U251 cells. In LN229 cells, Nrf2 expression rose at 1 μM but decreased as the concentration increased to 1.5 μM (Fig. 6b, f). HMOX1 reactivity increased at 1 μM in both cell types; however, its expression levels did not rise with higher concentrations (Fig. 6c, g). In LN229 cells, the expression of SOD1 showed enhanced reactivity at a concentration of 1 μM; however, further increases in concentration did not correspond to a continued increase in expression. In contrast, in U251 cells, SOD1 not only failed to show increased reactivity but also demonstrated inhibited expression at a concentration of 1.5 μM (Fig. 6d, h). The findings indicate that the intracellular antioxidant stress response system is activated at low concentrations of Celastrol, while its functionality is compromised at

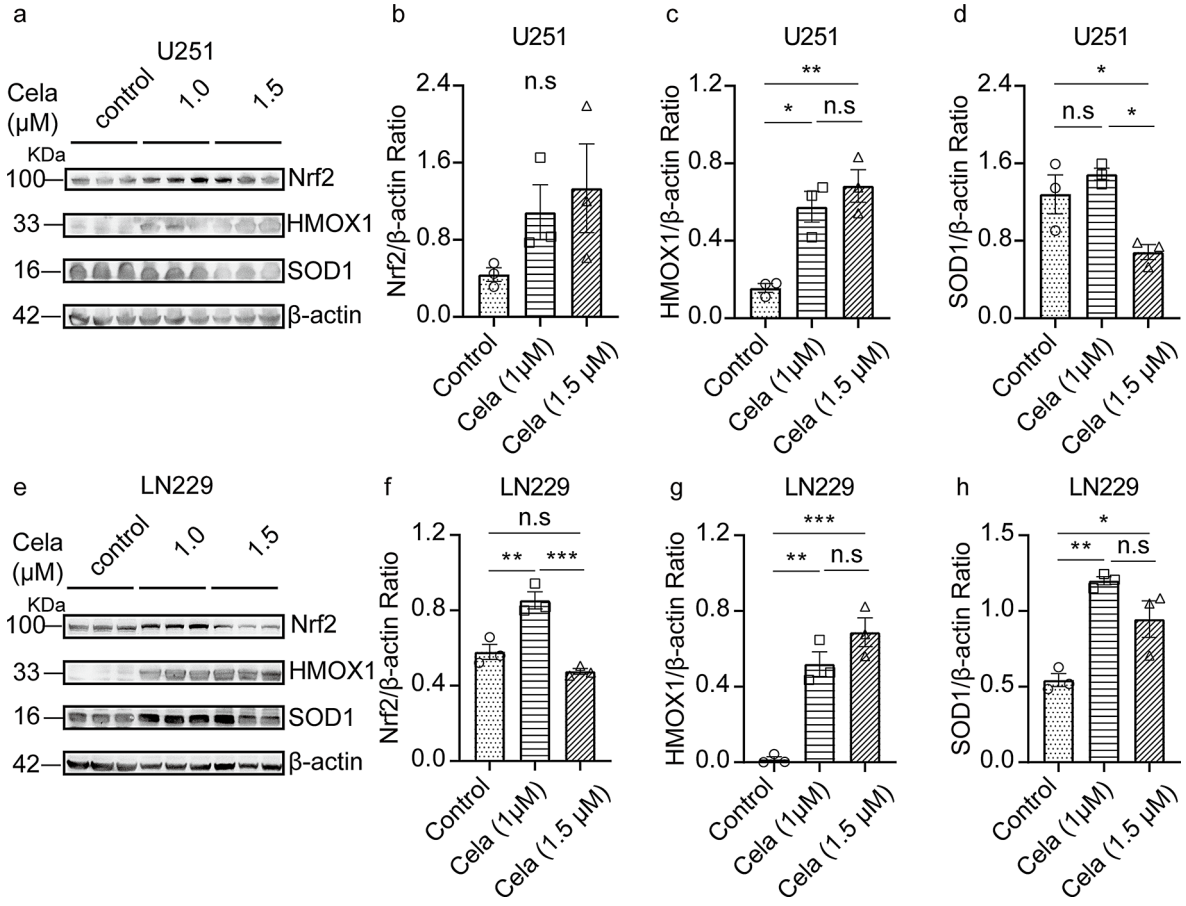


**Fig. 6** Effect of Celastrol on expression of antioxidant enzymes. (**a**, **e**) A representative Western blot analysis of Nrf2, HMOX1, and SOD1 in U251 and LN229 cell lysates. The cells were treated with Celastrol, and protein loading was normalized using β-actin as a control. (**b**, **c**, **d**) Quantifications of the protein expression levels shown in panel (a). (**f**, **g**, **h**) Quantifications of the data presented in panel (e). The data, based on three independent replicates, are expressed as the mean ± SEM and analyzed using one-way ANOVA. $^{*}p < 0.05$, $^{**}p < 0.01$, $^{***}p < 0.001$, $^{n.s}p > 0.05$. Abbreviation: Cela = Celastrol; HMOX1, heme oxygenase 1; SOD1, superoxide dismutase 1

higher concentrations. This alteration may be linked to the increased production of mitochondrial mROS at elevated concentrations.

In conclusion, high doses of Celastrol lead to an imbalance of mitochondrial redox homeostasis in human GBM cells.

### Celastrol restrains the proliferative capability of GBM cells by attenuating the expression levels of CDK1 and Cyclin B1

Mitochondrial dysfunction has been reported to inhibit the proliferation of tumor cells [33]. Based on the distinctive impacts of Celastrol on mitochondrial dynamics, function, redox homeostasis, and cell viability, our research further supports this idea. Since the mitotic cycle is controlled by the CDK1-Cyclin B1 complex, we examined how Celastrol affects the expression of Cyclin B1 and CDK1 at concentrations that promote mitochondrial fission. Western blot analysis showed that Celastrol treatment at 1 μM and 1.5 μM for 24 h reduced Cyclin B1 and CDK1 levels in U251 and LN229 cells (Fig. 7a, d). However, the inhibitory effect of Celastrol did not become stronger as the concentration increased (Fig. 7b, c, e, f). The findings suggest that Celastrol may exert an inhibitory effect on the proliferation of human GBM cells through the downregulation of the expression level of Cyclin B1 and CDK1.

### Celastrol inhibits GL261 growth and extends survival in GBM-bearing C57BL/6J mice

To examine Celastrol's effect on GBM cells in vivo, GL261 cells were used as the allograft cell line and C57BL/6J mice as the tumor-bearing models. The IC50 value for GL261 cells exposed to Celastrol for 24 h was determined to be 2.517 μM (Fig. 8a). Consistent with observations in human GBM cells, cell viability decreased in a concentration-dependent manner when Celastrol concentrations exceeded 1 μM (Fig. 8b). The colony formation assay demonstrated that exposure to 1 μM Celastrol for 8 h reduced the average colony-forming efficiency from 17 to 4% (Fig. 8c, d). These findings

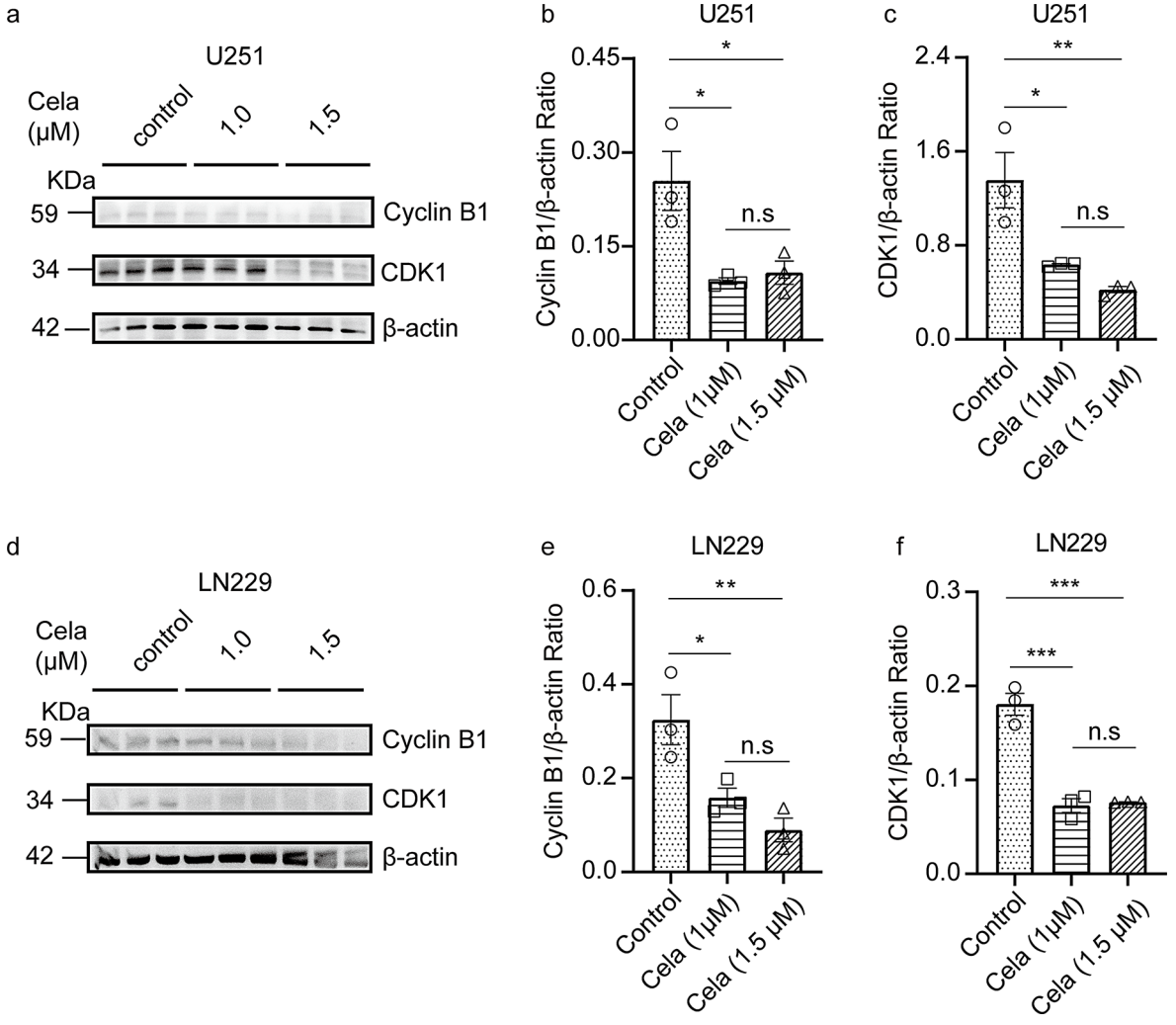


**Fig. 7** Celastrol inhibits the expression of Cyclin B1 and CDK1 in GBM cells. (**a**, **d**) Representative Western blot analysis of Cyclin B1 and CDK1 in U251 and LN229 cells lysates. The two cell lines were exposed to Celastrol (1 μM, 1.5 μM, 24 h). Protein loading was controlled with β-actin. (**b**, **c**, **e**, **f**) Quantifications of the protein expression levels shown in panel (a) and (d). The data from three independent replicates are expressed as the mean ± SEM and analyzed using one-way ANOVA. *$p < 0.05$, **$p < 0.01$, ***$p < 0.001$, $^{n.s}p > 0.05$. Abbreviation: Cela = Celastrol; CDK1 = cycle-dependent kinase 1

are similar to those observed in the colony formation of LN229 cells, indicating that Celastrol effectively inhibits GL261 cell proliferation in vitro. C57BL/6J mice were subcutaneously transplanted, administered, measured, and euthanized according to the experimental procedure (Fig. 8e). Tumor-bearing mice treated with Celastrol survived meaningfully longer than control mice. Mice in the control group had a median survival time of 7 days, while those treated with Celastrol had a median survival time of 18 days (Fig. 8f, g). These results suggest that Celastrol inhibits the proliferation of GL261 cells and extends the survival duration of C57BL/6J mice with GBM.

## Discussion

The prognosis for developing a cure for GBM, the most usual malignant neoplasm of the central nervous system, remains limited. Nevertheless, the good news is that anticancer schemes targeting mitochondrial dynamics have emerged as an encouraging treatment option. Therefore, the development of drugs that effectively target mitochondria has become one of the current research interests. Repurposing drugs from existing medicines will be a reasonable and cost-effective strategy [14]. Evidence indicates that Celastrol inhibits tumor growth in multiple cancers, such as GBM [16], lung and liver cancer [34, 35]. While limited research has examined Celastrol's impact on mitochondrial dynamics, numerous studies have shown that Celastrol increases intracellular ROS production and triggers cell cycle arrest and apoptosis through the ROS signaling pathway [16, 36]. Our work confirmed that Celastrol promoted mitochondrial fission in GBM cells. The main findings were shown in Fig. 9. In a study about non-small-cell lung cancer, the authors found that erastin synergizing with Celastrol

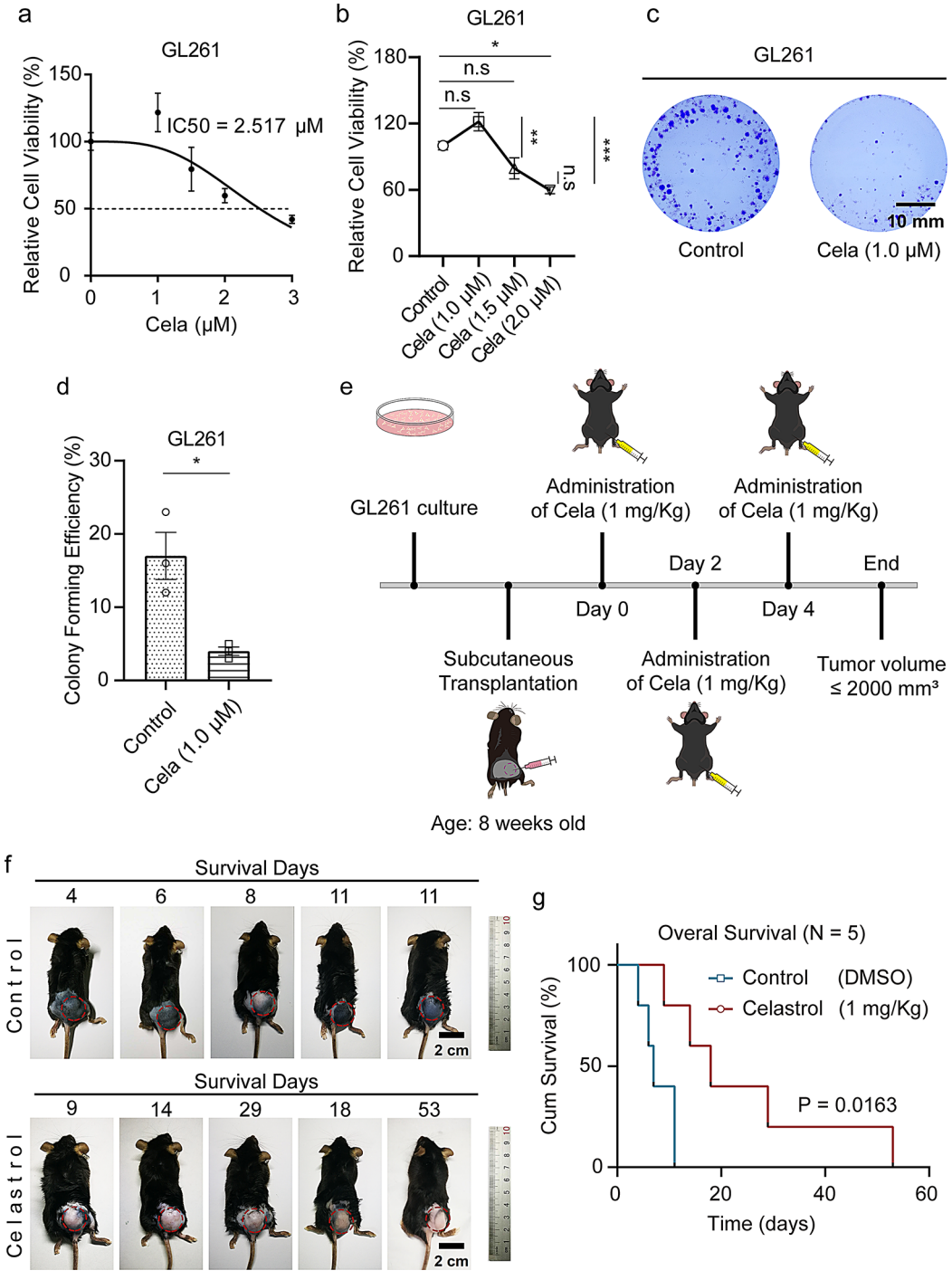


**Fig. 8** Celastrol inhibits GL261 growth and extends the survival of C57BL/6J mice with subcutaneous GBM. (**a**) IC50 curves of GL261 cells treated with Celastrol. (**b**) The effect of Celastrol on the viability of GL261 cells was assessed using the CCK-8 assay. Statistical analysis of the differences between groups was performed using a one-way ANOVA. $^{*}p < 0.05$, $^{**}p < 0.01$, $^{***}p < 0.001$, $^{n.s}p > 0.05$. Data are mean ± SEM. (**c**) Representative graphs of colony formation assay of GL261 treated with Celastrol (1 μM, 8 h). The scale bar represents a length of 10 mm. (**d**) Quantification of colony formation assay of GL261. Data are mean ± SEM. A two-tailed independent-sample t-test was employed. $^{*}p < 0.05$. (**e**) Schematic diagram of the experiment in vivo with mice. (**f**) Graphs of tumor-bearing mice treated without and with Celastrol (1 mg/Kg) and survival days of them. The scale bar represents a length of 2 cm. (**g**) Survival analysis of tumor-bearing mice. Data represent survival days of mice. Statistics of Kaplan-Meier curve was obtained using Log-rank Mantel-Cox test

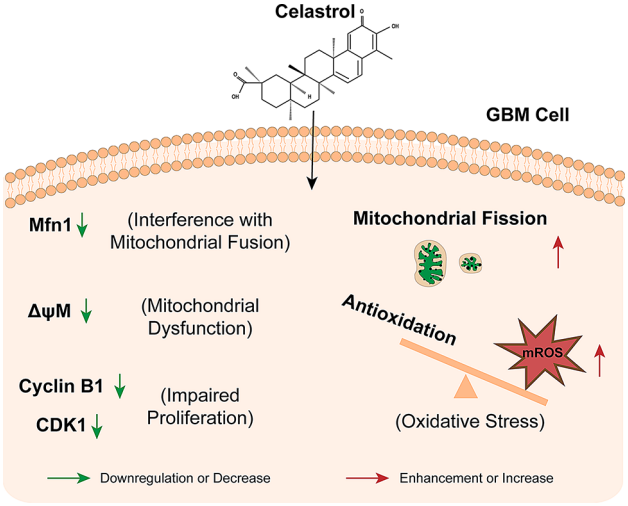


**Fig. 9** A schematic representation of the primary findings of the study. Celastrol facilitates mitochondrial fission through the suppression of Mfn1 expression in human GBM cells. Along with mitochondrial fission, a decline in ΔψM, oxidative stress, and decreased expression of Cyclin B1 and CDK1 are induced by Celastrol. These changes triggered by Celastrol may collectively inhibit the proliferation of GBM cells. Abbreviation: Mfn1 = mitofusin-1; ΔψM = mitochondrial membrane potential; CDK1 = Cyclin-dependent kinase 1

promoted mitochondrial fission at nontoxic concentrations. Even though they did not examine the individual effect of Celastrol on mitochondrial dynamics, their results likewise provided some support for our findings [19]. According to our research, Celastrol shows promise for repurposing as a therapy aimed at mitochondrial dynamics in GBM.

Most mitochondrial fusion and fission proteins reside in OMM, making it essential for mitochondrial dynamics. Mfn1 and Mfn2 facilitate OMM fusion, while Drp1, aided by receptors like MFF and Fis1, mediates OMM fission. In the OMM fusion reaction, Mfn1 is the central component [37], while Mfn2 is primarily involved in mitochondrial-ER interactions [38]. Most research about mitochondrial fission has focused on Drp1 [39], but this process is much more complex than the Drp1-mediated reaction. In addition to Drp1, its major receptors MFF and Fis1 also play important roles. As a result, the novel focus of our study was to observe the effects of Celastrol on the expression of Mfn1, MFF, and Fis1. Our results showed that the expression of Mfn1 was down-regulated at the concentrations of mitochondrial fission induced by Celastrol. Nevertheless, the expressions of MFF and Fis1 were not significantly affected by Celastrol at any concentration. Thereby, consistent with our results, we propose that the downregulation of Mfn1 suppresses mitochondrial fusion of OMM and promotes the transition of mitochondrial dynamics homeostasis towards fission. Moreover, we propose that Celastrol's effect on mitochondrial dynamics likely operates independently of MFF and Fis1. In a study on liver cancer, Li knocked out Mfn1 by sgRNA and subsequently found that mitochondria became significantly shorter [40]. This report further supports our viewpoint.

Interestingly, we found that Celastrol can not only disrupt the homeostasis of mitochondrial dynamics in human GBM cells at a concentration of only 1 μM but also remarkably reduce ΔψM. This means that Celastrol induces mitochondrial dysfunction while promoting mitochondrial fission. A study undertaken by Xv [41] elucidated various manifestations of mitochondrial dysfunction, including declined ΔψM and decreased ATP production following mitochondrial fission in vascular endothelial cells induced by Porphyromonas gingivalis infection. After blocking mitochondrial fission with Mdivi-1, mitochondrial dysfunction was reversed. This result is similar to what we found in our experiments. It is worth noting that in LN229 cells, mitochondrial fission was detected as early as 8 h after Celastrol treatment. This result indicates that the transition of mitochondrial dynamic homeostasis is one of the early responses of GBM cells to the injurious stimulus of Celastrol.

Our study demonstrated that the expression of antioxidant stress-related proteins (Nrf2, HMOX1, and SOD1) was upregulated at a Celastrol concentration of 1 μM. However, further increases in concentration to 1.5 μM did not enhance this upregulation, and there was a significant increase in mROS levels. Nrf2 regulates genes associated with detoxification enzymes and antioxidants, playing a key role in mitochondrial function and the control of ROS levels [42]. Upon elevation of Celastrol concentration, the expression of Nrf2 does not increase further and may even decrease, potentially contributing to the exacerbation of mitochondrial dysfunction and elevated levels of mROS. HMOX1, also referred to as heme oxygenase-1 (HO-1), serves as a downstream regulatory component within the Nrf2-ARE signaling pathway. Therefore, it is crucial to the anti-oxidative stress system. In a study of acute lung injury, Shi et al. reported that deficiency of HMOX1 not only intensified oxidative stress but also exacerbated mitochondrial fission [43]. SOD1, an antioxidative metalloenzyme, converts superoxide anion radicals into oxygen and hydrogen peroxide, maintaining the oxidation-antioxidant balance. According to Wang's report, SOD1 with dysfunction promotes mitochondrial fission and induces apoptosis [44]. A study on gastric cancer reported that Celastrol directly interacts with peroxoreductin-2 (PRDX2), resulting in the inhibition of its enzymatic activity and thereby increasing intracellular ROS [45]. Our comprehensive analysis suggests that Celastrol-induced oxidative stress in human GBM cells may involve the Nrf2-ARE-HMOX1 signaling pathway and direct inhibition of PRDX2 activity.

The morphology of mitochondria is intricately connected not only to energy metabolism but also to a variety of other cellular functions. Proper modulation of mitochondrial fission or fusion can facilitate the metabolic reprogramming of tumor cells, thereby promoting cell proliferation. Nevertheless, excessive mitochondrial fission can induce apoptosis [46]. Therefore, mitochondrial fission and fusion are crucial processes in regulating cell proliferation and the cell cycle [47, 48]. Our study found that Celastrol significantly reduces the expression of CDK1 and Cyclin B1 in GBM cells. This indicates that Celastrol not only disrupts the cell cycle but also has the potential to affect CDK1, as well as influence mitochondrial dynamics.

C57BL/6J mice, known for their robustness and easy care, are used in our study to assess Celastrol's therapeutic effects, setting a foundation for future in vivo research. Although Celastrol's ability to cross the blood-brain barrier is suggested, the exact penetration rate remains unknown. To bypass this barrier and facilitate observation, we used a subcutaneous GBM model, selecting GL261 as an allogeneic GBM cell line. Despite the biological differences between GL261 mouse-derived cells and human GBM cells, as well as the model's microenvironment differing from actual brain tissue—which limits its accuracy and relevance—the survival analysis results are consistent with Zhu et al.'s findings [49]. The anti-GBM effects of Celastrol, as demonstrated through both in vivo and in vitro experiments, suggest its potential for further development and research. Future studies will utilize immunodeficient mice to develop human GBM models, thereby enhancing simulation accuracy and reducing interference from the immune system. In addition, we'll use an orthotopic model to strengthen our argument and assess Celastrol's ability to cross the blood-brain barrier. While intraperitoneal injection offers a straightforward and convenient method for drug administration, its absorption is influenced by several factors, including the lipid solubility of the drug and the volume of fluid present in the abdominal cavity. In future research, we intend to explore intravenous drug administration to enhance the absorption rate of Celastrol and its effective distribution within tumor tissues.

In clinical settings, treatment failure and unfavorable prognosis in patients with GBM are frequently associated with the stem cell properties of the tumor [50]. The exclusion of glioma stem cells (GSCs) from research studies significantly diminishes the clinical translational relevance of the results. Therefore, future research endeavors should incorporate GSCs in in vitro studies to substantially enhance the translational value of the study.

Our study only preliminarily explored the pharmacological effects of Celastrol on mitochondrial dynamics, mitochondrial function, mitochondrial redox homeostasis, and cell proliferation. Due to limitations in research methods and resources, we couldn't thoroughly investigate the causal link between changes in mitochondrial dynamics and GBM cell proliferation, including the interaction between mitochondrial fission and cell cycle arrest. To elucidate the mechanisms, it is essential to further investigate additional pharmacological effects, including the post-translational modifications related to mitochondrial dynamin proteins and the characteristics of mitochondrial metabolism, in future studies. Furthermore, it is crucial to examine the role of Celastrol in the signaling pathways associated with oxidative stress, cell proliferation, and the cell cycle.

## Conclusion

In conclusion, we have presented evidence that Celastrol promotes mitochondrial fission in GBM cells by reducing Mfn1 expression. The excessive fission of mitochondria occurs alongside a decline in ΔψM, mitochondrial dysfunction, increased oxidative stress, and a reduction in CDK1 and Cyclin B1 expression. Our investigation reveals that Celastrol holds potential for repurposing as a therapeutic option targeting mitochondrial dynamics in GBM, deserving further research.

### Abbreviations

| | |
|---|---|
| CCK-8 | Cell Counting Kit-8 analysis |
| CDK1 | Cyclin-dependent kinase 1 |
| Cela | Celastrol |
| DMSO | Dimethyl sulfoxide |
| Drp-1 | Dynamin-related protein 1 |
| Fis1 | Fission 1 |
| GBM | Glioblastoma multiforme |
| GSCs | Glioma stem cells |
| HMOX1 | Heme oxygenase 1 |
| HO-1 | Haem oxygenase 1 |
| HRP | Horseradish peroxidase |
| MFF | Mitochondrial fission factor |
| Mfn1 | Mitofusin-1 |
| ΔψM | Mitochondrial membrane potential |
| mROS | Mitochondrial reactive oxygen species |
| Nrf2 | NF-E2-related factor 2 |
| OMM | Outer mitochondrial membrane |
| PRDX2 | Peroxoreductin-2 |
| ROS | Reactive oxygen species |
| SOD1 | Superoxide dismutase 1 |

## Supplementary Information

The online version contains supplementary material available at https://doi.org/10.1186/s12885-025-13733-9.

Supplementary Material 1

Supplementary Material 2

Supplementary Material 3

Supplementary Material 4

Supplementary Material 5

Supplementary Material 6

Supplementary Material 7

Supplementary Material 8

Supplementary Material 9

**Acknowledgements**
We extend our profound appreciation to Dr. Haima Li and Dr. Kai Sun for their invaluable contributions to the successful implementation of Western blot. We extend our sincere gratitude to Dr. Lei Guan for supporting the culture of GL261 cells.

**Author contributions**
J.Z.: conceptualization (lead), supervision (lead), validation (lead), review & editing (lead). L.L.: methodology (lead), investigation (lead), data curation (lead), formal analysis (lead), visualization (lead), and writing original draft (lead). W.L.: methodology (equal), resources (lead), data curation (equal), formal analysis (equal), and writing original draft (equal). G.C.: project administration (lead) and supervision (supporting). M.G.: conceptualization (supporting) and project administration (equal). J.S.: data curation (supporting) and resources (supporting). N.L. and H.Z.: investigation (supporting). B.G. and J.L.: review & editing (supporting). Y.L., S.X., J.W. and J.H.: resources (supporting).

**Funding**
This research was not funded by any public, commercial, or not-for-profit organizations.

**Data availability**
Upon reasonable request, the corresponding author is willing to deliver the data created and examined during this work.

## Declarations

**Consent for publication**
Not applicable.

**Competing interests**
The authors declare no competing interests.

**Author details**
[1]Medical School of Chinese PLA, Beijing 100853, China
[2]Department of Neurosurgery, Shanxi Bethune Hospital, Shanxi Academy of Medical Sciences, Third Hospital of Shanxi Medical University, Tongji Shanxi Hospital, Taiyuan 030032, China
[3]Department of Neurosurgery, The Sixth Medical Center of Chinese PLA General Hospital, Beijing 100048, China
[4]Department of Neurosurgery, The First Medical Center of Chinese PLA General Hospital, Beijing 100853, China
[5]Department of Neurosurgery, The Seventh Medical Center of Chinese PLA General Hospital, Beijing 100010, China
[6]Xiangyang Central Hospital, Xiangyang 441106, China

Received: 17 November 2024 / Accepted: 13 February 2025
Published online: 06 March 2025

**References**

1. Barnholtz-Sloan JS, Ostrom QT, Cote D. Epidemiology of brain tumors. Neurol Clin. 2018;36(3):395–419.
2. Ostrom QT, Price M, Neff C, Cioffi G, Waite KA, Kruchko C, Barnholtz-Sloan JS. CBTRUS Statistical Report: primary brain and other Central Nervous System tumors diagnosed in the United States in 2016–2020. Neuro Oncol. 2023;25(12 Suppl 2):iv1–99.
3. Janjua TI, Rewatkar P, Ahmed-Cox A, Saeed I, Mansfeld FM, Kulshreshtha R, Kumeria T, Ziegler DS, Kavallaris M, Mazzieri R, et al. Frontiers in the treatment of glioblastoma: past, present and emerging. Adv Drug Deliv Rev. 2021;171:108–38.
4. Monzel AS, Enríquez JA, Picard M. Multifaceted mitochondria: moving mitochondrial science beyond function and dysfunction. Nat Metab. 2023;5(4):546–62.
5. Wai T, Langer T. Mitochondrial dynamics and metabolic regulation. Trends Endocrinol Metab. 2016;27(2):105–17.
6. Wang Y, Liu HH, Cao YT, Zhang LL, Huang F, Yi C. The role of Mitochondrial Dynamics and Mitophagy in Carcinogenesis, Metastasis and Therapy. Front Cell Dev Biol. 2020;8:413.
7. Missiroli S, Perrone M, Genovese I, Pinton P, Giorgi C. Cancer metabolism and mitochondria: finding novel mechanisms to fight tumours. EBioMedicine. 2020;59:102943.
8. Mohamed Yusoff AA. Role of mitochondrial DNA mutations in brain tumors: a mini-review. J Cancer Res Ther. 2015;11(3):535–44.
9. Iranmanesh Y, Jiang B, Favour OC, Dou Z, Wu J, Li J, Sun C. Mitochondria's role in the maintenance of Cancer Stem cells in Glioblastoma. Front Oncol. 2021;11:582694.
10. Ghosh P, Vidal C, Dey S, Zhang L. Mitochondria Targeting as an effective strategy for Cancer Therapy. Int J Mol Sci. 2020;21(9).
11. Mukherjee S, Bhatti GK, Chhabra R, Reddy PH, Bhatti JS. Targeting mitochondria as a potential therapeutic strategy against chemoresistance in cancer. Biomed Pharmacother. 2023;160:114398.
12. Gatto L, Di Nunno V, Ghelardini A, Tosoni A, Bartolini S, Asioli S, Ratti S, Di Stefano AL, Franceschi E. Targeting Mitochondria in Glioma: new hopes for a cure. Biomedicines. 2024;12(12).
13. Wang N, Huang R, Yang K, He Y, Gao Y, Dong D. Interfering with mitochondrial dynamics sensitizes glioblastoma multiforme to temozolomide chemotherapy. J Cell Mol Med. 2022;26(3):893–912.
14. Jin P, Jiang J, Zhou L, Huang Z, Nice EC, Huang C, Fu L. Mitochondrial adaptation in cancer drug resistance: prevalence, mechanisms, and management. J Hematol Oncol. 2022;15(1):97.
15. Wang C, Dai S, Zhao X, Zhang Y, Gong L, Fu K, Ma C, Peng C, Li Y. Celastrol as an emerging anticancer agent: current status, challenges and therapeutic strategies. Biomed Pharmacother. 2023;163:114882.
16. Liu X, Zhao P, Wang X, Wang L, Zhu Y, Song Y, Gao W. Celastrol mediates autophagy and apoptosis via the ROS/JNK and Akt/mTOR signaling pathways in glioma cells. J Exp Clin Cancer Res. 2019;38(1):184.
17. Zhu Y, Liu X, Zhao P, Zhao H, Gao W, Wang L. Celastrol suppresses glioma vasculogenic mimicry formation and angiogenesis by blocking the PI3K/Akt/mTOR signaling pathway. Front Pharmacol. 2020;11:25.
18. Cha Z, Cheng J, Xiang H, Qin J, He Y, Peng Z, Jia J, Yu H. Celastrol enhances TRAIL-induced apoptosis in human glioblastoma via the death receptor pathway. Cancer Chemother Pharmacol. 2019;84(4):719–28.
19. Liu M, Fan Y, Li D, Han B, Meng Y, Chen F, Liu T, Song Z, Han Y, Huang L, et al. Ferroptosis inducer erastin sensitizes NSCLC cells to celastrol through activation of the ROS-mitochondrial fission-mitophagy axis. Mol Oncol. 2021;15(8):2084–105.
20. Franken NA, Rodermond HM, Stap J, Haveman J, van Bree C. Clonogenic assay of cells in vitro. Nat Protoc. 2006;1(5):2315–9.
21. Valente AJ, Maddalena LA, Robb EL, Moradi F, Stuart JA. A simple ImageJ macro tool for analyzing mitochondrial network morphology in mammalian cell culture. Acta Histochem. 2017;119(3):315–26.
22. Yang R, Gao W, Wang Z, Jian H, Peng L, Yu X, Xue P, Peng W, Li K, Zeng P. Polyphyllin I induced ferroptosis to suppress the progression of hepatocellular carcinoma through activation of the mitochondrial dysfunction via Nrf2/HO-1/GPX4 axis. Phytomedicine. 2024;122:155135.
23. Ito S, Araya J, Kurita Y, Kobayashi K, Takasaka N, Yoshida M, Hara H, Minagawa S, Wakui H, Fujii S, et al. PARK2-mediated mitophagy is involved in regulation of HBEC senescence in COPD pathogenesis. Autophagy. 2015;11(3):547–59.
24. Oh T, Fakurnejad S, Sayegh ET, Clark AJ, Ivan ME, Sun MZ, Safaee M, Bloch O, James CD, Parsa AT. Immunocompetent murine models for the study of glioblastoma immunotherapy. J Transl Med. 2014;12:107.
25. Diao C, Yang Z, Hu Q, Yao P, Qu X, Li C, Zhang S, Zhou J. Celastrol alleviates mitochondrial oxidative stress and brain Injury after Intracerebral Hemorrhage by promoting OPA1-Dependent mitochondrial Fusion. Neuroscience. 2024;536:79–91.
26. Stribbling SM, Ryan AJ. The cell-line-derived subcutaneous tumor model in preclinical cancer research. Nat Protoc. 2022;17(9):2108–28.
27. Giacomello M, Pyakurel A, Glytsou C, Scorrano L. The cell biology of mitochondrial membrane dynamics. Nat Rev Mol Cell Biol. 2020;21(4):204–24.
28. Chan DC. Mitochondrial dynamics and its involvement in Disease. Annu Rev Pathol. 2020;15:235–59.
29. Willems PH, Rossignol R, Dieteren CE, Murphy MP, Koopman WJ. Redox Homeostasis and mitochondrial dynamics. Cell Metab. 2015;22(2):207–18.

30. Hraoui G, Grondin M, Breton S, Averill-Bates DA. Nrf2 mediates mitochondrial and NADPH oxidase-derived ROS during mild heat stress at 40°C. Biochim Biophys Acta Mol Cell Res. 2025;1872(3):119897.
31. Cheung EC, Vousden KH. The role of ROS in tumour development and progression. Nat Rev Cancer. 2022;22(5):280–97.
32. Chadha S, Behl T, Kumar A, Khullar G, Arora S. Role of Nrf2 in rheumatoid arthritis. Curr Res Transl Med. 2020;68(4):171–81.
33. Ruocco MR, Avagliano A, Granato G, Vigliar E, Masone S, Montagnani S, Arcucci A. Metabolic flexibility in melanoma: a potential therapeutic target. Semin Cancer Biol. 2019;59:187–207.
34. Si H, Wang H, Xiao H, Fang Y, Wu Z. Anti-tumor Effect of Celastrol on Hepatocellular Carcinoma by the circ_SLIT3/miR-223-3p/CXCR4 Axis. Cancer Manag Res. 2021;13:1099–111.
35. Yan YF, Zhang HH, Lv Q, Liu YM, Li YJ, Li BS, Wang PY, Shang WJ, Yue Z, Xie SY. Celastrol suppresses the proliferation of lung adenocarcinoma cells by regulating microRNA-24 and microRNA-181b. Oncol Lett. 2018;15(2):2515–21.
36. Moreira H, Szyjka A, Paliszkiewicz K, Barg E. Prooxidative Activity of Celastrol Induces Apoptosis, DNA Damage, and Cell Cycle Arrest in Drug-Resistant Human Colon Cancer Cells. Oxid Med Cell Longev. 2019:6793957.
37. Ishihara N, Eura Y, Mihara K. Mitofusin 1 and 2 play distinct roles in mitochondrial fusion reactions via GTPase activity. J Cell Sci. 2004;117(Pt 26):6535–46.
38. Naón D, Hernández-Alvarez MI, Shinjo S, Wieczor M, Ivanova S, Martins de Brito O, Quintana A, Hidalgo J, Palacín M, Aparicio P, et al. Splice variants of mitofusin 2 shape the endoplasmic reticulum and tether it to mitochondria. Science. 2023;380(6651):eadh9351.
39. Chen P, Lu Y, He B, Xie T, Yan C, Liu T, Wu S, Yeh Y, Li Z, Huang W, et al. Rab32 promotes glioblastoma migration and invasion via regulation of ERK/Drp1-mediated mitochondrial fission. Cell Death Dis. 2023;14(3):198.
40. Li S, Han S, Zhang Q, Zhu Y, Zhang H, Wang J, Zhao Y, Zhao J, Su L, Li L, et al. FUNDC2 promotes liver tumorigenesis by inhibiting MFN1-mediated mitochondrial fusion. Nat Commun. 2022;13(1):3486.
41. Xu T, Dong Q, Luo Y, Liu Y, Gao L, Pan Y, Zhang D. Porphyromonas gingivalis infection promotes mitochondrial dysfunction through Drp1-dependent mitochondrial fission in endothelial cells. Int J Oral Sci. 2021;13(1):28.
42. Payandeh Z, Pirpour Tazehkand A, Barati G, Pouremamali F, Kahroba H, Baradaran B, Samadi N. Role of Nrf2 and mitochondria in cancer stem cells; in carcinogenesis, tumor progression, and chemoresistance. Biochimie. 2020;179:32–45.
43. Shi J, Yu T, Song K, Du S, He S, Hu X, Li X, Li H, Dong S, Zhang Y et al. Dexmedetomidine ameliorates endotoxin-induced acute lung injury in vivo and in vitro by preserving mitochondrial dynamic equilibrium through the HIF-1a/HO-1 signaling pathway. Redox Biol 2021;41:101954.
44. Wang H, Yi J, Li X, Xiao Y, Dhakal K, Zhou J. ALS-associated mutation SOD1(G93A) leads to abnormal mitochondrial dynamics in osteocytes. Bone. 2018;106:126–38.
45. Chen X, Zhao Y, Luo W, Chen S, Lin F, Zhang X, Fan S, Shen X, Wang Y, Liang G. Celastrol induces ROS-mediated apoptosis via directly targeting peroxiredoxin-2 in gastric cancer cells. Theranostics. 2020;10(22):10290–308.
46. Wu Z, Xiao C, Li F, Huang W, You F, Li X. Mitochondrial fusion-fission dynamics and its involvement in colorectal cancer. Mol Oncol. 2024;18(5):1058–75.
47. Dong F, Zhu M, Zheng F, Fu C. Mitochondrial fusion and fission are required for proper mitochondrial function and cell proliferation in fission yeast. Febs j. 2022;289(1):262–78.
48. Dubal D, Moghe P, Verma RK, Uttekar B, Rikhy R. Mitochondrial fusion regulates proliferation and differentiation in the type II neuroblast lineage in Drosophila. PLoS Genet. 2022;18(2):e1010055.
49. Zhu S, Sun F, Zhao P, Liang G, Sun X, Zeng L, Huang Y. Brain-targeting biomimetic nanoparticles for codelivery of celastrol and LY2157299 for reversing glioma immunosuppression. Int J Pharm. 2022;619:121709.
50. Eckerdt F, Platanias LC. Emerging role of glioma stem cells in mechanisms of Therapy Resistance. Cancers. 2023;15(13):3458.

## Publisher's note